Letter | Editors' Suggestion

Transverse voltage in anisotropic hydrodynamic conductors

Kaize Wang [1,*] Chunyu Guo [1] Philip J. W. Moll [1,†] and Tobias Holder [2,‡]
[1]*Max Planck Institute for the Structure and Dynamics of Matter, Hamburg 22761, Germany*
[2]*School of Physics and Astronomy, Tel Aviv University, Tel Aviv 69978, Israel*

(Received 13 August 2024; revised 9 December 2024; accepted 13 January 2025; published 6 February 2025)

Weak momentum dissipation in ultraclean metals gives rise to novel non-Ohmic current flow, including ballistic and hydrodynamic regimes. Recently, hydrodynamic flow has attracted intense interest because it presents a valuable window into the electronic correlations and the longest lived collective modes of quantum materials. However, diagnosing viscous flow is difficult as the macroscopic observables of ballistic and hydrodynamic transport such as the average current distribution can be deceptively similar, even if their respective microscopics deviate notably. Based on kinetic Boltzmann theory, here we propose to address this issue via the transverse channel voltage at zero magnetic field, which can efficiently detect hydrodynamic flow in a number of materials. To this end, we show that the transverse voltage is sensitive to the interplay between anisotropic fermiology and boundary scattering, resulting in a nontrivial behavior in narrow channels along crystalline low-symmetry directions. We discuss several materials where the channel-size dependent stress of the quantum fluid leads to a characteristic sign change of the transverse voltage as a new hallmark of the crossover from the ballistic to the hydrodynamic regime.

DOI: 10.1103/PhysRevB.111.L081402

Introduction. Hy drodynamic electron flow is a special transport regime which onsets when a rapid electron-electron scattering rate exceeds all other relaxation mechanisms. In recent years, its fundamental importance became apparent in understanding the longest lived collective modes of correlated electrons [1–4]. For example, viscous (hydrodynamic) correlations can shed light on electronic collective behavior, on the interacting phase diagram, and reveal unusual characteristics in the electron dynamics [5–7]. Hydrodynamic electron flow has also been discussed in connection to THz electromagnetic radiation in transistors [8–10], ambipolar transports in semiconductors/semimetals [11–13], and fluid spintronics [14–17]. The current conceptual frontiers of interacting Fermi liquids are found in understanding correlations on the nanoscale, either due to extreme scattering rates in strongly correlated electron systems such as high-T_c superconductors, or due to nanoconfinement in heterostructures such as the nanoscopic channel sizes of current transistors. Advancing these goals necessitates experimental approaches sensing momentum diffusion in confined conductors. The last few years saw tremendous experimental progress in the imaging [18–23] and characterization [4,24–26] of the crossover regime between hydrodynamic and ballistic flow. At the same time, these efforts have revealed that the flow profile of a quantum fluid in thin channels is rather ambiguous with respect to the dominant relaxation mechanism [27]. While it is possible to alleviate this issue by choosing other geometries [21,28–30] or measure at finite magnetic field [31,32], identifying more accessible characteristics sensitive to the ballistic-hydrodynamic crossover is highly sought after. The key point of this letter is to establish the transverse channel voltage in anisotropic conductors as such an accessible characteristic.

Electron transport in mesoscopic conductors is characterized by three characteristic length scales [33]: The system size W, the momentum-relaxing (MR) mean-free path ℓ_{mr}, and the momentum-conserving (MC) mean-free path ℓ_{mc}. In very clean systems it holds that $W \ll \ell_{\mathrm{mr}}$ and Ohm's law no longer describes the local relationship between electric field and current. The system therefore becomes ballistic [34] if $W \ll \ell_{\mathrm{mr}} \ll \ell_{\mathrm{mc}}$ or hydrodynamic if $\ell_{\mathrm{mc}} \ll W \ll \ell_{\mathrm{mr}}$ [Fig. 1(a)]. The physical tuning knob for ℓ_{mc} is usually temperature, which controls the underlying dominant microscopic scattering mechanism [19,35–39]. This mechanism can involve either nonumklapp electron-electron scattering or boson-mediated electron-electron interactions.

In previous studies, the crossover regime (Gurzhi regime) when all three length scales are comparable ($W \approx \ell_{\mathrm{mr}} \approx \ell_{\mathrm{mc}}$) has been studied theoretically by a Boltzmann kinetic approach with a Callaway two-rate ansatz for isotropic Fermi surfaces [32,33,40,41]. The implicit assumption for this starting point is that the simplified isotropic description ought to capture the qualitative features of the ballistic-hydrodynamic crossover. However, this is far from obvious: Experimentally, it is important to investigate the sensitivity of observables such as flow profiles against inevitable misalignments between the channel and the crystal axes. Since several candidate materials with hydrodynamic electronic transport

*Contact author: kaize.wang@mpsd.mpg.de
†Contact author: philip.moll@mpsd.mpg.de
‡Contact author: tobiasholder@tauex.tau.ac.il

Published by the American Physical Society under the terms of the Creative Commons Attribution 4.0 International license. Further distribution of this work must maintain attribution to the author(s) and the published article's title, journal citation, and DOI. Open access publication funded by Max Planck Society.

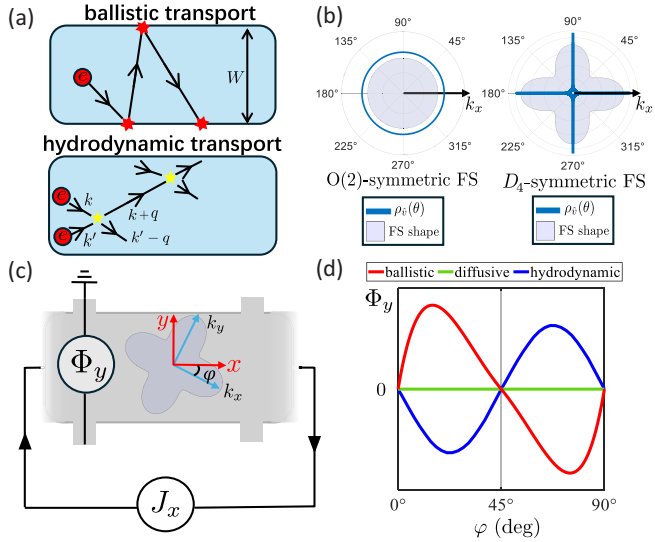


FIG. 1. (a) Ballistic and hydrodynamic transport regimes. (b) Representative FS with continuous rotational symmetry and with anisotropy. $\rho_{\hat{v}}$ denotes the distribution of Fermi velocity directions, shown in a polar histogram. (c) A four point geometry for measurements of transverse voltages with misalignment angle φ between the crystal principle axis and the channel direction. (d) Expected transverse voltage as a function of misalignment angle for a FS with D_4 symmetry.

are in fact metals with anisotropic Fermi surfaces [19,24,42], it is critical to investigate the effect of symmetry breaking through the channel walls on hydrodynamic flow. Conversely, the Fermi surface (FS) shape can provide valuable insight for the ballistic-hydrodynamic crossover. Theoretical efforts to explore anisotropic effects in hydrodynamic conductors include broadband microwave spectroscopy [43,44], a non-monotonic temperature and width dependence of the channel conductance [45], and viscous flow profiles on a Corbino disk [46].

Here, we address this question by examining the transverse voltage in the absence of magnetic field. Our main focus is anisotropic systems [Fig. 1(b)] lacking mirror symmetry due to a directional mismatch between the high symmetry axis of the FS and the geometric axis of the channel [Fig. 1(c)]. To describe these systems, we generalize the Callaway ansatz, finding a transverse voltage at zero magnetic field which is strongly sensitive to the microscopic scattering mechanism. Depending on the FS shape, a sign reversal of this transverse voltage can indicate that the system crosses over from ballistic to hydrodynamic flow [Fig. 1(d)]. We identify this strong dependence on the MC scattering rate as a competition of the transverse stress induced by the boundaries against the stress resulting from the bulk MR scattering. Using the sign to identify the onset of hydrodynamic regimes offers several advantages. Firstly, it only requires a nonspatially resolved transport measurement of a single device. Secondly, the sign change of the transverse voltage is uncommon outside the hydrodynamic context, as it typically only relates to the carrier type of the material. However, we remark that the sign change does not mark a precise boundary point between the ballistic and hydrodynamic regimes.

Collisional invariants for anisotropic Fermi surfaces. We aim to describe the ballistic-hydrodynamic crossover using semiclassical kinetics. The starting point is the Boltzmann transport equation (BTE) for the distribution function f, given by $(\partial_t + \mathbf{v_k}\cdot\nabla_\mathbf{r} + \mathbf{F}\cdot\nabla_\mathbf{k})f(\mathbf{r},\mathbf{p},t) = C[f(\mathbf{r},\mathbf{p},t)]$, where C is the collision integral and $\mathbf{F}$ is the perturbation. The deviation from the equilibrium state is linearized by writing $f(\mathbf{r},\mathbf{p},t) - f^0(\varepsilon_\mathbf{p}) = -E_F\partial_\varepsilon f^0(\epsilon)h(\mathbf{r},\mathbf{p},t)$, where E_F is the Fermi energy and h is dimensionless nonequilibrium distribution function. In the following, we consider the low temperature limit where $\partial_\varepsilon f^0(\varepsilon) \approx -\delta(\epsilon - E_F)$, suitable for materials with a large carrier density. For the sake of simplicity, we consider a single FS for which a bijection between angular variable θ and Fermi wave vector $\mathbf{p}_F$ exits. This allows to integrate out the radial momentum dependence of $\mathbf{p}$, leaving only an angular momentum variable θ. In more general scenarios, the FS arclength should be employed for each Fermi pocket separately, followed by a sum over multiple FSs.

We begin by defining a bra-ket notation for the BTE [43,45,47]. Let $g(\mathbf{r},\theta,t)$ be a state function on the FS. Then the corresponding ket and inner product in two dimensions are defined by $|g(\mathbf{r},t)\rangle = \int d\theta\sqrt{A(\theta)}g(\mathbf{r},\theta,t)|\theta\rangle$ where $\langle\theta|\theta'\rangle = \delta(\theta-\theta')$ and the metric in phase space is $A(\theta) = p_F^2(\theta)E_F/(2\pi\hbar)^2|\mathbf{v}_F(\theta)\cdot\mathbf{p}_F(\theta)|$. With this definition, $\langle g(\mathbf{r},t)\rangle = \langle h(\mathbf{r},t)|g(\mathbf{r},t)\rangle$. We define the following modes with unit length: A particle mode called $|c\rangle \propto \int d\theta\sqrt{A(\theta)}|\theta\rangle$, corresponding to the particle number, and a momentum mode called $|p_\mu\rangle \propto \int d\theta\sqrt{A(\theta)}p_\mu(\theta)|\theta\rangle$, relevant for contractions which preserve momentum [24,33,43,45,47,48].

To proceed, we take the Callaway two-rate ansatz [40] for the collision integral C. The main idea is to restrict C to a small set of longest-lived eigenmodes. For electron flow in a channel, these modes derive from particle number, which is conserved exactly; and momentum, which relaxes with a small scattering rate $\gamma_{\rm mr}$. We note that the assumption of isotropic scattering rates is approximate and most well-suited for weakly correlated materials which are good conductors [49]. Assuming that all other excitations relax at least as fast as these quasiconserved quantities with rate $\gamma = \gamma_{\rm mc} + \gamma_{\rm mr}$ [43,45], one obtains two collisional integrals,

$$C_{\rm mr} = -\gamma_{\rm mr}(\mathbb{1} - |c\rangle\langle c|),$$
$$C_{\rm mc} = -\gamma_{\rm mc}\left(\mathbb{1} - |c\rangle\langle c| - \sum_\mu |p_\mu\rangle\langle p_\mu|\right). \quad (1)$$

As long as $W \ll v_F/\gamma_{\rm mr}$, this construction guarantees both particle number and (approximate) momentum conservation since $\langle c|C_{\rm mr/mc}|h\rangle = 0$ and $\langle p_\mu|C_{\rm mc}|h\rangle = 0$.

Consider the current flow in a long narrow channel geometry (Fig. 1) at zero magnetic field and zero temperature, which is translationally invariant in the longitudinal direction (denoted x). Therefore, the distribution function only has a spatial dependence in y direction. As a function of the two parameters (y,θ), the BTE becomes

$$D[h] = (C_{\rm mr} + C_{\rm mc})|h\rangle, \quad (2)$$

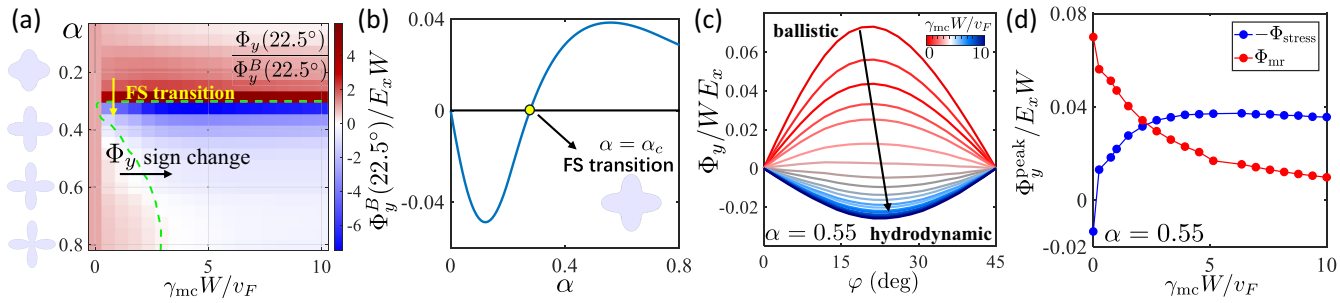


FIG. 2. (a) Transverse voltage at 22.5° normalized by the ballistic value, shown as a function of both FS anisotropy α and dimensionless MC rate. Green dotted line: Interpolated boundary line when transverse voltage is vanishing. Yellow arrow: FS transition at $\alpha \approx 0.3$, corresponding to a sign-change of ballistic transverse voltage, black arrow: A line-cut for a fixed FS, where transverse voltage changes sign with increase MC rate. (b) Ballistic transverse voltage as a function of α. Yellow dot: nontrivial zero of the ballistic transverse voltage signifying the FS transition. (c) Transverse voltage as a function of misalignment angle φ, parameters are taken as indicated by the black line cut in (a). From ballistic to hydrodynamic region, the transverse voltage flips its sign. (d) Decomposition of the transverse voltage. As MC rate increases, MR contribution is decreasing to zero and the stress component is dominant.

where the drift terms are $D[h] = \partial_y|v_y h\rangle - E_x|v_x\rangle - E_y|v_y\rangle$. Here, E_x, E_y are electric fields normalized by the Fermi energy, having the unit of a wave vector. The longitudinal electric field E_x is fixed, while $E_y(y)$ is determined self-consistently. Rearranging terms, one obtains

$$C_0|h\rangle = \sum_\mu E_\mu|v_\mu\rangle + \left[\gamma|c\rangle\langle c| + \gamma_{\rm mc}\sum_\nu |p_\nu\rangle\langle p_\nu|\right]|h\rangle, \quad (3)$$

where $C_0|h\rangle = \partial_y|v_y h\rangle + \gamma|h\rangle$. A diffusive boundary condition is imposed as [33,50] $h^\pm(\mp W/2,\theta) = 0$ and $J_y(y) \equiv \langle v_y|h\rangle = 0$. Here, $h^\pm(y,\theta)$ are $h(y,\theta)$ restricted to the domain $\Theta^\pm = \{\theta|\text{sign}[v_y(\theta)] = \pm 1\}$, respectively.

In this form, we can solve the BTE self-consistently and obtain the transverse electric field as $E_y(y) = \langle p_y|v_y\rangle^{-1}(\langle p_y|C_0|h\rangle - \gamma_{\rm mc}\sum_\mu \langle h|p_\mu\rangle\langle p_\mu|v_y\rangle)$. The transverse voltage is the integral $\Phi_y = \int dy\, E_y(y)$. We identify two different mechanisms in Φ_y, originating from the stress due to ohmic dissipation and viscous dissipation, respectively. Denoting $\Phi_y = \Phi_y^{\rm stress} + \Phi_y^{\rm mr}$, it is

$$\Phi_y^{\rm stress} = \langle p_y|v_y\rangle^{-1}\langle p_y|v_y h\rangle\big|_{-W/2}^{W/2}$$
$$\Phi_y^{\rm mr} = \langle p_y|v_y\rangle^{-1}\gamma_{\rm mr}\int_{-W/2}^{W/2} dy\langle p_y|h\rangle. \quad (4)$$

Here, $\Phi_y^{\rm stress}$ is related to the yy component of the stress tensor $\Pi_{\mu\nu} \equiv \langle p_\mu|v_\nu h\rangle$ of the quantum fluid [53,54], whereas $\Phi_y^{\rm mr}$ is proportional to the MR rate $\gamma_{\rm mr}$.

Ballistic-hydrodynamic crossover. In order to demonstrate the anisotropy effect of FSs in a tractable manner, we use the following parametrization for the Fermi wave vector k_F for a D_n FS $k_F(\theta;\alpha,\varphi) = k_F^0\{1 + \alpha\cos[n(\theta-\varphi)]\}$, where θ is the angle between $\mathbf{k}_F$ and the crystal k_x-axis, φ is the angle between the crystal and channel axes as shown in Fig. 2(a). α is the controlling parameter for the FS shape. With varying α, the FS goes from circular to cross-shaped, and finally flower-shaped, as shown in Fig. 2(a) for $n = 4$.

Focusing on the non-Ohmic region, we fix the MR rate $\gamma_{\rm mr}$ within the limit $\gamma_{\rm mr}W/v_F \lesssim 1$ and change the MC rate $\gamma_{\rm mc}$ to investigate the ballistic-hydrodynamic crossover. The transverse voltage at the misalignment angle $\varphi = 22.5°$ (i.e., maximal misalignment) as a function of both FS shape and MC scattering rate is shown in Fig. 2(a). In order to track the sign change of the transverse voltage, we normalize by the ballistic voltage Φ_B with $\gamma_{\rm mc} = 0$. For a fixed small $\alpha < \alpha_c$, the transverse voltage remains of the same sign irrespective of the value of $\gamma_{\rm mc}$. At the critical value $\alpha_c \approx 0.3$, the increasingly anisotropic FS leads to a sign change of the ballistic voltage (yellow arrow). Such a sign reversal is a direct consequence of the Fermi velocity distribution of different FSs, which is the only relevant factor in the ballistic limit. In the Supplemental Material [48], we elucidate that this latter sign change is determined by the average $\langle v_x \text{sign}(v_y)\rangle$.

In contrast, for a fixed large $\alpha > \alpha_c$, with increasing MC scattering rate $\gamma_{\rm mc}$, the voltage exhibits an additional sign change between the ballistic region and the hydrodynamic region [cf. green dotted line in Fig. 2(a)]. This latter sign change persists for all misalignment angles, as is shown in Fig. 2(c). Thus, during the ballistic-hydrodynamic crossover, certain anisotropic FSs will cause the modulus of the transverse voltage to decrease, cross zero smoothly and change sign. Note that $\Phi_y(\varphi)$ can have a quite asymmetric shape, changing noticeably as a function of $\gamma_{\rm mc}$. To investigate the origin of the transverse voltage, $\Phi_y^{\rm stress}$ and $\Phi_y^{\rm mr}$ [Eq. (4)] are shown in Fig. 2(d) for the anisotropy parameter $\alpha = 0.55$. Φ_y here is taken as the peak voltage in the whole range of φ rotation at a fixed $\gamma_{\rm mr}$ and varying with $\gamma_{\rm mc}$. We observe that in the hydrodynamic regime ($\gamma_{\rm mc}W/v_F \gg 1$), the MR component is vanishing so that the internal stress of the quantum fluid becomes the dominant contribution to the transverse voltage. Conversely, the dissipative stress dominates at small $\gamma_{\rm mc}$, therefore there exists a critical $\gamma_{\rm mc}^c$ where the two contributions cancel and the sign of transverse voltage Φ_y reverses.

Material examples. Here we present some instructive examples of anisotropic FSs which additionally contain anisotropic Fermi velocities. We find that both a continuum model and tight-binding (TB) examples can exhibit a behavior very similar to the one discussed for the sim-

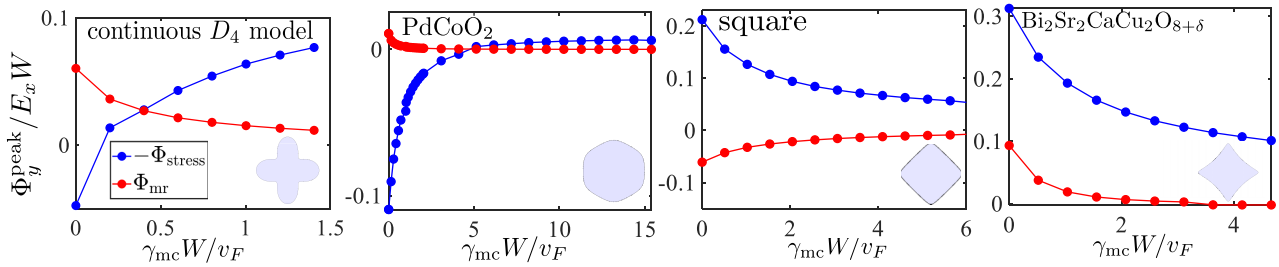


FIG. 3. Decomposition of the transverse voltage of different models. Left to right: D_4 model with a energy dispersion $\varepsilon(k)$ with $\gamma_{\rm mr}W/v_F = 0.1$ [48], TB model for $PdCoO_2$ [51] with $\gamma_{\rm mr}W/v_F = 0.08$, TB square model with $\gamma_{\rm mr}W/v_F = 0.49$ [48],TB model for overdoped cuprate Bi2212 [52] with $\gamma_{\rm mr}W/v_F = 0.49$. Inset: Fermi surface shapes of different models.

plified scenario, thus confirming the robustness of our diagnosis. Namely, we focus on the ultra clean material $PdCoO_2$ [24], and the overdoped strongly correlated cuprate $Bi_2Sr_2CaCu_2O_{8+\delta}$(Bi2212) [42], as in both non-Ohmic transport has been observed. For comparison, we also include a square lattice with nearest-neighbor hopping. The model details can be found in the Supplemental Material [48], the results of these calculations are shown in Fig. 3. Not surprisingly, in all cases the MR component is diminishing when approaching the hydrodynamic limit. Thus in the hydrodynamic region, the only contribution to transverse voltage is the yy component of the stress tensor $\Pi_{\mu\nu}$. For the anisotropic D_4 model [48], our calculation reveals a sign change of the transverse voltage with increasing MC scattering rate, serving as a direct indicator of hydrodynamic transport. The location of this crossover, however, depends on the FS shape, the channel width, and the el-el scattering rate. For the FSs of the square and Bi2212, for example, such a sign change would occur only at extreme scattering rates. Thus in a real material, these parameters may render the sign change inaccessible for realistic channel sizes.

The diagnostic methodology can be extended to treat those situations, thus greatly expanding its range of applicability. The transverse voltage results from a competition between $\Phi_y^{\rm stress}$ and $\Phi_y^{\rm mr}$, which in general scale differently with the channel misalignment angle φ [see asymmetry evolution in Fig. 2(c)]. Hence, the transverse voltage difference between two channels symmetrically misaligned by an angle $\pm\delta\varphi$ to mutually adjacent mirror planes is a sensitive probe of emergent hydrodynamics (Fig. 4). Its asymmetry is actually most pronounced in the weakly hydrodynamic sector of small $\gamma_{\rm mc}W/v_F$ and a channel width dependence allows an estimation of $\gamma_{\rm mc}$ through a transport experiment. The required simple geometry of two canted bars is sketched in Fig. 4(a). Varying the channel width by a factor of 10 is straightforward lithographically, which will provide enough range to extract γ_{mc} even when the sign change itself cannot be accessed.

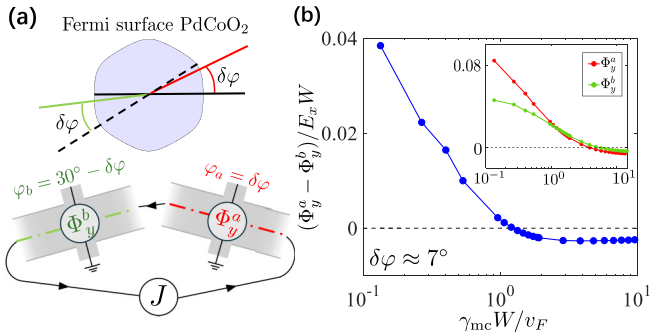


FIG. 4. (a) Sketch for measurement of the difference of transverse voltage $\Phi_y^a - \Phi_y^b$ at misalignment angle $\varphi_a = \delta\varphi$ and $\varphi_b = 30° - \delta\varphi$ for $PdCoO_2$. (b) Difference of transverse voltage as function of MC scattering rate. Inset: Φ_y^a and Φ_y^b as a function of MC scattering rate.

Conclusion. By employing a Callaway two-rate ansatz, we have identified a nonvanishing transverse voltage for a wide range of low-symmetry transport configurations. We find that in a D_4-symmetric system, a sufficiently anisotropic FS can lead to a sign change in the transverse voltage as the electron fluid crosses over from ballistic to hydrodynamic transport. We therefore propose that measuring the transverse voltage at zero magnetic field can be a viable way to distinguish different types of non-Ohmic transport. The prescribed phenomenology offers an alternative probe for the experimental investigation of unconventional charge transport beyond the analysis of the current flow pattern. We reiterate that the measurement of transverse voltage seems particularly attractive because it does not require an external magnetic field or a local imaging of the current profile. We believe that the sign change is observable with current devices as a function of either gate voltage or temperature using the geometry depicted in Fig. 4. For example, in Ref. [24], the estimated range of $\gamma_{\rm mr}/\gamma_{\rm mc}$ is $0.05 \sim 0.2$, based on fits of the conductivity to an isotropic model.

As a limitation of our results, we note that the simplifications to the collision integral employed in this work cannot adequately capture the intermediate tomographic transport regime [47,55–57]. The methodology developed here can be straightforwardly extended to investigate hydrodynamic crossovers in three-dimensional systems. Another promising direction for future work is the study of magneto-transport in anisotropic systems.

Acknowledgments. T.H. acknowledges financial support by the European Research Council (ERC) under grant Quantum-CUSP (Grant Agreement No. 101077020).

[1] A. Lucas and K. Chung Fong, Hydrodynamics of electrons in graphene, J. Phys.: Condens. Matter **30**, 053001 (2018).

[2] B. N. Narozhny, Hydrodynamic approach to two-dimensional electron systems, Riv. Nuovo Cim. **45**, 661 (2022).

[3] G. Varnavides, A. Yacoby, C. Felser, and P. Narang, Charge transport and hydrodynamics in materials, Nat. Rev. Mater. **8**, 726 (2023).

[4] L. Fritz and T. Scaffidi, Hydrodynamic electronic transport, Annu. Rev. Condens. Matter Phys. **15**, 17 (2024).

[5] P. K. Kovtun, D. T. Son, and A. O. Starinets, Viscosity in strongly interacting quantum field theories from black hole physics, Phys. Rev. Lett. **94**, 111601 (2005).

[6] B. N. Narozhny and A. Levchenko, Coulomb drag, Rev. Mod. Phys. **88**, 025003 (2016).

[7] S. A. Hartnoll, A. Lucas, and S. Sachdev, *Holographic Quantum Matter* (MIT Press, Cambridge, MA, 2018).

[8] J. H. Farrell, N. Grisouard, and T. Scaffidi, Terahertz radiation from the Dyakonov-Shur instability of hydrodynamic electrons in Corbino geometry, Phys. Rev. B **106**, 195432 (2022).

[9] J. Crabb, X. Cantos-Roman, J. M. Jornet, and G. R. Aizin, Hydrodynamic theory of the Dyakonov-Shur instability in graphene transistors, Phys. Rev. B **104**, 155440 (2021).

[10] M. Dyakonov and M. Shur, Shallow water analogy for a ballistic field effect transistor: New mechanism of plasma wave generation by dc current, Phys. Rev. Lett. **71**, 2465 (1993).

[11] C. Tan, D. Y. H. Ho, L. Wang, J. I. A. Li, I. Yudhistira, D. A. Rhodes, T. Taniguchi, K. Watanabe, K. Shepard, P. L. McEuen, C. R. Dean, S. Adam, and J. Hone, Dissipation-enabled hydrodynamic conductivity in a tunable bandgap semiconductor, Sci. Adv. **8**, eabi8481 (2022).

[12] Y. Nam, D.-K. Ki, D. Soler-Delgado, and A. F. Morpurgo, Electron–hole collision limited transport in charge-neutral bilayer graphene, Nat. Phys. **13**, 1207 (2017).

[13] C. A. Kukkonen and P. F. Maldague, Electron-hole scattering and the electrical resistivity of the semimetal TiS_2, Phys. Rev. Lett. **37**, 782 (1976).

[14] M. Matsuo, Y. Ohnuma, and S. Maekawa, Theory of spin hydrodynamic generation, Phys. Rev. B **96**, 020401 (2017).

[15] R. Takahashi, M. Matsuo, M. Ono, K. Harii, H. Chudo, S. Okayasu, J. Ieda, S. Takahashi, S. Maekawa, and E. Saitoh, Spin hydrodynamic generation, Nat. Phys. **12**, 52 (2016).

[16] R. Takahashi, H. Chudo, M. Matsuo, K. Harii, Y. Ohnuma, S. Maekawa, and E. Saitoh, Giant spin hydrodynamic generation in laminar flow, Nat. Commun. **11**, 3009 (2020).

[17] G. Tatara, Hydrodynamic theory of vorticity-induced spin transport, Phys. Rev. B **104**, 184414 (2021).

[18] M. J. H. Ku, T. X. Zhou, Q. Li, Y. J. Shin, J. K. Shi, C. Burch, L. E. Anderson, A. T. Pierce, Y. Xie, A. Hamo, U. Vool, H. Zhang, F. Casola, T. Taniguchi, K. Watanabe, M. M. Fogler, P. Kim, A. Yacoby, and R. L. Walsworth, Imaging viscous flow of the Dirac fluid in graphene, Nature (London) **583**, 537 (2020).

[19] U. Vool, A. Hamo, G. Varnavides, Y. Wang, T. X. Zhou, N. Kumar, Y. Dovzhenko, Z. Qiu, C. A. C. Garcia, A. T. Pierce, J. Gooth, P. Anikeeva, C. Felser, P. Narang, and A. Yacoby, Imaging phonon-mediated hydrodynamic flow in WTe_2, Nat. Phys. **17**, 1216 (2021).

[20] L. Ella, A. Rozen, J. Birkbeck, M. Ben-Shalom, D. Perello, J. Zultak, T. Taniguchi, K. Watanabe, A. K. Geim, S. Ilani, and J. A. Sulpizio, Simultaneous imaging of voltage and current density of flowing electrons in two dimensions, Nat. Nanotechnol. **14**, 480 (2019).

[21] C. Kumar, J. Birkbeck, J. A. Sulpizio, D. Perello, T. Taniguchi, K. Watanabe, O. Reuven, T. Scaffidi, A. Stern, A. K. Geim, and S. Ilani, Imaging hydrodynamic electrons flowing without Landauer-Sharvin resistance, Nature (London) **609**, 276 (2022).

[22] A. Aharon-Steinberg, A. Marguerite, D. J. Perello, K. Bagani, T. Holder, Y. Myasoedov, L. S. Levitov, A. K. Geim, and E. Zeldov, Long-range nontopological edge currents in charge-neutral graphene, Nature (London) **593**, 528 (2021).

[23] A. Jenkins, S. Baumann, H. Zhou, S. A. Meynell, Y. Daipeng, K. Watanabe, T. Taniguchi, A. Lucas, A. F. Young, and A. C. Bleszynski Jayich, Imaging the breakdown of ohmic transport in graphene, Phys. Rev. Lett. **129**, 087701 (2022).

[24] P. J. W. Moll, P. Kushwaha, N. Nandi, B. Schmidt, and A. P. Mackenzie, Evidence for hydrodynamic electron flow in $PdCoO_2$, Science **351**, 1061 (2016).

[25] N. Nandi, T. Scaffidi, P. Kushwaha, S. Khim, M. E. Barber, V. Sunko, F. Mazzola, P. D. C. King, H. Rosner, P. J. W. Moll, M. König, J. E. Moore, S. Hartnoll, and A. P. Mackenzie, Unconventional magneto-transport in ultrapure $PdCoO_2$ and $PtCoO_2$, npj Quantum Mater. **3**, 66 (2018).

[26] J. Gooth, F. Menges, N. Kumar, V. Süß, C. Shekhar, Y. Sun, U. Drechsler, R. Zierold, C. Felser, and B. Gotsmann, Thermal and electrical signatures of a hydrodynamic electron fluid in tungsten diphosphide, Nat. Commun. **9**, 4093 (2018).

[27] J. A. Sulpizio, L. Ella, A. Rozen, J. Birkbeck, D. J. Perello, D. Dutta, M. Ben-Shalom, T. Taniguchi, K. Watanabe, T. Holder, R. Queiroz, A. Principi, A. Stern, T. Scaffidi, A. K. Geim, and S. Ilani, Visualizing Poiseuille flow of hydrodynamic electrons, Nature (London) **576**, 75 (2019).

[28] A. Aharon-Steinberg, T. Völkl, A. Kaplan, A. K. Pariari, I. Roy, T. Holder, Y. Wolf, A. Y. Meltzer, Y. Myasoedov, M. E. Huber, B. Yan, G. Falkovich, L. S. Levitov, M. Hücker, and E. Zeldov, Direct observation of vortices in an electron fluid, Nature (London) **607**, 74 (2022).

[29] A. Stern, T. Scaffidi, O. Reuven, C. Kumar, J. Birkbeck, and S. Ilani, How electron hydrodynamics can eliminate the Landauer-Sharvin resistance, Phys. Rev. Lett. **129**, 157701 (2022).

[30] D. A. Bandurin, A. V. Shytov, L. S. Levitov, R. K. Kumar, A. I. Berdyugin, M. Ben Shalom, I. V. Grigorieva, A. K. Geim, and G. Falkovich, Fluidity onset in graphene, Nat. Commun. **9**, 4533 (2018).

[31] Y. Huang and M. Wang, Nonnegative magnetoresistance in hydrodynamic regime of electron fluid transport in two-dimensional materials, Phys. Rev. B **104**, 155408 (2021).

[32] T. Scaffidi, N. Nandi, B. Schmidt, A. P. Mackenzie, and J. E. Moore, Hydrodynamic electron flow and Hall viscosity, Phys. Rev. Lett. **118**, 226601 (2017).

[33] M. J. M. de Jong and L. W. Molenkamp, Hydrodynamic electron flow in high-mobility wires, Phys. Rev. B **51**, 13389 (1995).

[34] In this paper, the term ballistic transport refers specifically to the bulk properties of the material. It does not imply the absence of boundary scattering, which is assumed to be diffusive in our formalism.

[35] R. N. Gurzhi, Reviews of topical problems: Hydrodynamic effects in solids at low temperature, Sov. Phys. Usp. **11**, 255 (1968).

[36] P. Heilmann, P. V. Pyshkin, and B. Trauzettel, Transition between scattering regimes of two-dimensional electron transport, Phys. Rev. B **110**, 115420 (2024).

[37] A. Jaoui, B. Fauqué, C. W. Rischau, A. Subedi, C. Fu, J. Gooth, N. Kumar, V. Süß, D. L. Maslov, C. Felser, and K. Behnia, Departure from the Wiedemann-Franz law in WP_2 driven by mismatch in T-square resistivity prefactors, npj Quantum Mater. **3**, 64 (2018).

[38] A. Jaoui, B. Fauqué, and K. Behnia, Thermal resistivity and hydrodynamics of the degenerate electron fluid in antimony, Nat. Commun. **12**, 195 (2021).

[39] A. Jaoui, A. Gourgout, G. Seyfarth, A. Subedi, T. Lorenz, B. Fauqué, and K. Behnia, Formation of an electron-phonon bifluid in bulk antimony, Phys. Rev. X **12**, 031023 (2022).

[40] J. Callaway, Model for lattice thermal conductivity at low temperatures, Phys. Rev. **113**, 1046 (1959).

[41] T. Holder, R. Queiroz, T. Scaffidi, N. Silberstein, A. Rozen, J. A. Sulpizio, L. Ella, S. Ilani, and A. Stern, Ballistic and hydrodynamic magnetotransport in narrow channels, Phys. Rev. B **100**, 245305 (2019).

[42] J. Zaanen, Planckian dissipation, minimal viscosity and the transport in cuprate strange metals, SciPost Phys. **6**, 061 (2019).

[43] G. Baker, D. Valentinis, and A. P. Mackenzie, On non-local electrical transport in anisotropic metals, Low Temp. Phys. **49**, 1338 (2023).

[44] G. Baker, T. W. Branch, J. S. Bobowski, J. Day, D. Valentinis, M. Oudah, P. McGuinness, S. Khim, P. Surówka, Y. Maeno, T. Scaffidi, R. Moessner, J. Schmalian, A. P. Mackenzie, and D. A. Bonn, Nonlocal electrodynamics in ultrapure $PdCoO_2$, Phys. Rev. X **14**, 011018 (2024).

[45] C. Q. Cook and A. Lucas, Electron hydrodynamics with a polygonal Fermi surface, Phys. Rev. B **99**, 235148 (2019).

[46] G. Varnavides, A. S. Jermyn, P. Anikeeva, C. Felser, and P. Narang, Electron hydrodynamics in anisotropic materials, Nat. Commun. **11**, 4710 (2020).

[47] P. J. Ledwith, H. Guo, and L. Levitov, The hierarchy of excitation lifetimes in two-dimensional Fermi gases, Ann. Phys. **411**, 167913 (2019).

[48] See Supplemental Material at http://link.aps.org/supplemental/10.1103/PhysRevB.111.L081402 for further details on the derivation of the Boltzmann kinetic approach for anisotropic Fermi surfaces, the transverse voltage decomposition, as well as various model systems discussed in the main text.

[49] M. D. Bachmann, A. L. Sharpe, G. Baker, A. W. Barnard, C. Putzke, T. Scaffidi, N. Nandi, P. H. McGuinness, E. Zhakina, M. Moravec, S. Khim, M. König, D. Goldhaber-Gordon, D. A. Bonn, A. P. Mackenzie, and P. J. W. Moll, Directional ballistic transport in the two-dimensional metal $PdCoO_2$, Nat. Phys. **18**, 819 (2022).

[50] E. I. Kiselev and J. Schmalian, Boundary conditions of viscous electron flow, Phys. Rev. B **99**, 035430 (2019).

[51] H. Takatsu, J. J. Ishikawa, S. Yonezawa, H. Yoshino, T. Shishidou, T. Oguchi, K. Murata, and Y. Maeno, Extremely large magnetoresistance in the nonmagnetic metal $PdCoO_2$, Phys. Rev. Lett. **111**, 056601 (2013).

[52] R. S. Markiewicz, S. Sahrakorpi, M. Lindroos, H. Lin, and A. Bansil, One-band tight-binding model parametrization of the high-T_c cuprates including the effect of k_z dispersion, Phys. Rev. B **72**, 054519 (2005).

[53] B. Bradlyn, M. Goldstein, and N. Read, Kubo formulas for viscosity: Hall viscosity, Ward identities, and the relation with conductivity, Phys. Rev. B **86**, 245309 (2012).

[54] P. Massignan, G. M. Bruun, and H. Smith, Viscous relaxation and collective oscillations in a trapped Fermi gas near the unitarity limit, Phys. Rev. A **71**, 033607 (2005).

[55] J. Hofmann and U. Gran, Anomalously long lifetimes in two-dimensional Fermi liquids, Phys. Rev. B **108**, L121401 (2023).

[56] S. Kryhin and L. Levitov, Collinear scattering and long-lived excitations in two-dimensional electron fluids, Phys. Rev. B **107**, L201404 (2023).

[57] Q. Hong, M. Davydova, P. J. Ledwith, and L. Levitov, Superscreening by a retroreflected hole backflow in tomographic electron fluids, Phys. Rev. B **109**, 085126 (2024).